YORP Effect on Asteroid 162173 Ryugu: Implications for the Dynamical History

M. Kanamaru[1], S. Sasaki[2], T. Morota[3], Y. Cho[3], E. Tatsumi[4], M. Hirabayashi[5], N. Hirata[6], H. Senshu[7], Y. Shimaki[1], N. Sakatani[8], S. Tanaka[1], T. Okada[1], T. Usui[1], S. Sugita[3], S. Watanabe[9].

[1]Institute of Space and Astronautical Science (ISAS), Japan Aerospace Exploration Agency (JAXA), 3-3-1 Yoshinodai, Sagamihara 252-5210, Japan.
[2]Osaka University, 1-1 Machikaneyama, Toyonaka, Osaka 560-0043, Japan.
[3]The University of Tokyo, 7-3-1 Hongo, Bunkyo, Tokyo 1130033, Japan.
[4]Instituto de Astrofísica de Canarias, C/Vía Láctea, 38205 La Laguna - Tenerife - España.
[5]Auburn University, 211 Davis Hall, Auburn, AL 36849-5338, United States
[6]University of Aizu, Tsuruga, Ikkimachi, Aizu Wakamatsu, Fukushima 965-8580, Japan.
[7]Chiba Institute of Technology, 2-17-1 Tsudanuma, Narashino, Chiba 275-0016, Japan.
[8]Rikkyo University, 3-34-1 Nishi-Ikebukuro, Toshima, Tokyo 171-8501, Japan.
[9]Nagoya University, Furo-cho, Chikusa-ku, Nagoya, Aichi 464-8601 Japan.

Key Points:

- Thermal recoil torque (i.e., the YORP effect) plays a dominant role in the spin-down of asteroid 162173 Ryugu.
- The estimated spin-down time scale (0.58 – 8.7 million years) indicates a period of major change in the topography of Ryugu.
- The YORP effect is responsible for keeping the spin-pole of Ryugu perpendicular to the orbital plane.

Corresponding author: Masanori Kanamaru, `kanamaru.masanori@jaxa.jp`

Abstract

Asteroid 162173 (Ryugu) is a carbonaceous asteroid that was visited by Japan's Hayabusa2 spacecraft in 2018. The formation mechanism of spinning-top shape of Ryugu is an essential clue to the dynamical history of the near-Earth asteroid. In this study, we address the long-term evolution of the spin state of Ryugu induced by the Yarkovsky–O'Keefe–Radzievskii–Paddack (YORP) effect, i.e., the thermal recoil torque that changes the rotation period and spin-pole direction.

Given the current orbit, spin state, and three-dimensional shape observed by Hayabusa2, we computed the YORP torque exerted on Ryugu using a simplified thermal model approximating zero thermal conductivity. Despite differences in meter-scaled topography, all 20 shape models that we examined indicate that the spin velocity of Ryugu is currently decreasing at a rate of $(-0.42 - -6.3) \times 10^{-6}$ deg/day^2. Our findings also suggest that the thermal torque on the asteroid is responsible for maintaining the spin pole upright with respect to the orbital plane.

Therefore, the YORP effect could explain the significant spin-down from a period of 3.5 h initially to 7.6 h currently. The corresponding time scale of the rotational deceleration is estimated to be 0.58 – 8.7 million years, depending on the input shape models. This time scale is comparable to e.g., the formation period of the largest crater, *Urashima* (5 – 12 Ma) or the western bulge (2 – 9 Ma) as derived from previous studies on crater statistics in Ryugu. It is considered that the rotation of the asteroid started to decelerate in the wake of the major crater formation or the resurfacing event on the western hemisphere.

Plain Language Summary

The Japanese spacecraft Hayabusa2 visited the kilometer-sized asteroid, Ryugu, and found it to have a spinning-top shape with a diamond-like cross section. For an aggregate of rock fragments to deform in this way, fast rotation is required. The rotation period of Ryugu is 7.6 h, and its rotational speed is not sufficiently fast to deform the entire body. It is proposed that Ryugu initially spun rapidly and has since slowed down. Light has no mass, but it does have momentum and produces a faint pressure. As the asteroid is heated from the Sun, radiation is emitted from the asteroid surface, resulting in a breaking effect and changing the rotational speed of the asteroid over millions of years. We found that the

radiation pressure is a reasonable mechanism for the spin-down of the asteroid and thus provides a clue to Ryugu's history.

1 Introduction

Japan's Hayabusa2 was a sample return mission from the C-type near-Earth asteroid, 162173 (1999 JU_3) Ryugu (Tachibana et al., 2014; Watanabe et al., 2017; Tsuda et al., 2019). The Hayabusa2 spacecraft arrived at the target asteroid in June 2018 and started its homeward journey to Earth in November 2019 after an approximately 17-month asteroid-proximity phase. The mission included two successful touchdowns to sample the surface material, an artificial cratering experiment, and deployment of a lander and rovers. Hayabusa2 revealed the nature of the rocky surface and its spinning-top shape (Watanabe et al., 2019). The spinning-top-shaped body has an elevated ridge in the equatorial region and a flat cross section in the mid-latitude region, unlike spherical or ellipsoidal objects. Ryugu's shape is considered to be the result of deformation induced by fast rotation in the past (Watanabe et al., 2019). According to finite-element-method analysis Hirabayashi et al. (2019), a fast rotation at a period of approximately 3.0 – 3.5 h is sufficient to induce interior structural failure or surface mass wasting due to centrifugal force. However, the spin-down process from the past rapid rotation to the current milder state (7.6 h period) remains unknown. The goal of this study is to explore the Yarkovsky–O'Keefe—Radzievskii–Paddack (YORP) effect on Ryugu, i.e., thermally induced spin alteration (Rubincam, 2000), which is one of the greatest contributors to the spin dynamics of the asteroid. We propose a new approach to reveal its evolutionary history by combining a dynamical simulation and analyses of geologic features. The dynamical process sensitive to a topographic change enables us to integrate the two perspectives.

1.1 Asteroid Ryugu revealed by Hayabusa2

We present a brief review of the scientific achievements of Hayabusa2 at the time of writing. Watanabe et al. (2019) is a flagship report on the first impression of Ryugu, including the spinning-top shape as mentioned above. The spinning-top shape and rocky surface strongly suggested that Ryugu is a rubble pile formed by the catastrophic disruption of a parent body and reaccumulation of the fragments. For our later simulations, we utilized the orbital elements, rotation period, spin-pole orientation, and other physical properties of Ryugu reported in this study (see Table 1). Ryugu is a retrograde rotator with a pole almost perpendicular to its orbital plane, for which the obliquity ε (i.e., tilt angle of the spin axis with respect to the normal vector of a body's orbital plane) corresponds to 171.6°.

Table 1. Properties of asteroid 162173 Ryugu in the J2000.0 frame at the epoch of 2018 July 1.0 TDB (See the supplementary material of Watanabe et al. (2019)).

Parameters	Notation	Value	Unit
Orbital elements			
Semi-major axis	a	1.190	AU
Eccentricity	e	0.1903	–
Inclination	I	5.884	deg
Longitude of ascending node	Ω	251.6	deg
Argument of perihelion	ω	211.4	deg
Mean anomaly	Φ	21.94	deg
Rotation pole and period			
Right ascension (RA)	α	96.40	deg
Declination (Dec)	δ	-66.40	deg
Ecliptic longitude	λ	179.3	deg
Ecliptic latitude	β	-87.44	deg
Obliquity	ε	171.6	deg
Rotation period	P	7.633	h
Physical properties			
GM	GM	30.0	m^3/s^2
Mass	M	4.50×10^{11}	kg
Volume	V	0.377 ± 0.005	km^3
Mean density	ρ	$1{,}190 \pm 20$	kg/m^3

Three-dimensional (3D) shape models of Ryugu were constructed from images captured by the onboard optical navigation camera (ONC) and have been updated until the time of writing. In the Hayabusa2 project, two different methods are used for 3D shape reconstruction: stereo-photoclinometry (SPC) (R. Gaskell et al., 2006; R. W. Gaskell et al., 2008) and structure-from-motion (SfM) (Szeliski, 2011). Ryugu's volume, as derived from the shape model and mass from spacecraft tracking data during a descent operation onto the asteroid, yielded a bulk density of 1190 ± 20 kg/m^3 (Watanabe et al., 2019). The average reflectance spectrum of Ryugu is very flat from visible to near-infrared wavelengths, and its geometric albedo is very low, i.e., $4.0 \pm 0.5\%$ at the 0.55 µm band (Tatsumi et al., 2020). The reflectance spectrum can be classified as Cb-type in the Bus and Binzel taxonomy (Sugita et al., 2019) and C/F-type in the Tholen taxonomy (Tatsumi et al., 2020). A weak but sharp absorption feature at 2.72 µm was detected across the entire surface. These features suggest that, similar to the heated Ivuna meteorite, Ryugu is composed of CM- or CI-like materials (Kitazato et al., 2019). Because the bulk density of Ryugu is smaller than that of many types of carbonaceous chondrites, the porosity of Ryugu could exceed 50% (Watanabe et al., 2019).

Global ONC observations of Ryugu revealed many of its geologic properties, including an east-west dichotomy, an equatorial ridge, numerous impact craters, and a high abundance of large boulders (Sugita et al., 2019). Closer examinations of surface features on Ryugu show evidence of mass motion from the equatorial ridges toward mid-latitude regions, such as imbricated boulders and regolith run-ups on the ridge sides of boulders. Such direction of mass motion is consistent with geopotential changes due to the spin deceleration of Ryugu; a decrease in centrifugal force increases the geopotential of the equatorial ridge and lowers that of mid-latitude regions (Sugita et al., 2019; Morota et al., 2020). Global mapping also revealed that the surface of Ryugu exhibits distinctive latitudinal color variation that supports the deceleration-induced mass motion. The most prominent color variation in visible wavelengths is observed in the spectral slope between the b- and x-bands (0.48–0.86 µm) (Sugita et al., 2019; Tatsumi et al., 2020). The variation in the b–x spectral slope is correlated with the geopotential (or elevation measured from an equipotential surface). Areas of high potential, such as the polar and equatorial regions, tend to have smaller or negative b-x slopes (i.e., bluer spectra). In contrast, the mid-latitude areas of Ryugu have positive b-x slopes (i.e., redder spectra). This color variation suggests that materials weathered on the surface migrate from highlands to lowlands in response to the current shape and gravity field of Ryugu; this is likely caused by the most recent major mass motion on Ryugu (Sugita et al., 2019). Thus, both morphological and spectral surface features on Ryugu support the recent deceleration in spin rate.

Further, crater statistics can serve as indicators for the surface age of a solid objects and the mechanical properties of the surface layer. Hirata et al. (2020) provided a comprehensive list of impact craters larger than 20 m on Ryugu and discussed their spatial distribution. More detailed morphological studies of the craters are reported in Noguchi et al. (2021). A statistical randomness analysis by Hirata et al. (2020) confirmed that those craters are concentrated in the equatorial region (30°S–30°N) rather than follow a random distribution. Moreover, the number density of the craters varies longitudinally. The so-called western bulge (160°E–290°E) has fewer craters than regions around the prime meridian of Ryugu (300°E − 30°E). Additionally, Michikami et al. (2019) reported a difference in boulder abundance (> 5 m) between the eastern and western hemispheres. In fact, the number density of the boulders is relatively lower in the western hemisphere. The origin of the western bulge is proposed to be a past deformation process of Ryugu during a period of fast rotation (Hirabayashi et al., 2019) or regolith landslides toward the western side at a rapid spin (Scheeres, 2015). These processes could resurface in the western hemisphere of Ryugu and result in an east–west dichotomy in the crater and boulder densities. Ryugu's craters were also found to possess morphological features, such as raised rims and wall slumping, consistent with unconsolidated surface materials. Based on this observation, Sugita et al. (2019) estimated the residence time of Ryugu in the main asteroid belt since the formation of the current topography to be 8.9 ± 2.5 Ma using the gravity scaling rule for coarse-grain targets (Tatsumi & Sugita, 2018). The use of gravity-scaling was subsequently validated by the artificial impact experiment conducted by Hayabusa2 (Arakawa et al., 2020).

Based on detailed crater observations using close-up images, Morota et al. (2020) found that Ryugu experienced orbital excursion toward the Sun after leaving a stable orbit in the main belt. This sunward orbital excursion likely reddened the surface layer (≤ 1 m) through solar heating and/or solar wind irradiation. Crater counting indicates that the surface reddening event was terminated at 0.3 to 8.1 Ma. Because the erosion of the red surface layer through the despinning-induced mass motion postdates the reddening event, it can be deduced that the rotational deceleration of Ryugu has likely occurred in the last 0.3 − 8.1 Ma.

1.2 Observational and theoretical studies on YORP

Spin parameters of asteroids have been actively investigated through light curve and radar observation. However, to detect a secular change in the rotation period, multiple observation sessions over several years are required. The YORP effect was initially detected by the increase in the spin velocity of asteroid 54509 YORP (2000 PH5) (Lowry et al., 2007; Taylor et al., 2007). Since then, YORP-induced spin-up has been observed in several sub-kilometer-sized asteroids: 1862 Apollo (Kaasalainen et al., 2007; Ďurech, Vokrouhlický, Kaasalainen, Weissman, et al., 2008), 1620 Geographos (Ďurech, Vokrouhlický, Kaasalainen, Higgins, et al., 2008), 3103 Eger (Ďurech et al., 2012, 2018), 25143 Itokawa (Lowry et al., 2014), 1685 Toro (Ďurech et al., 2018), and 161989 Cacus (Ďurech et al., 2018). Most recently, asteroid 101955 Bennu was observed to be spinning up at a rate of $(3.63 \pm 0.52) \times 10^{-6}$ deg/day^2 by ground-based observations and NASA's OSIRIS-REx spacecraft (Nolan et al., 2019; Hergenrother et al., 2019). Although the rotation period of asteroid 162173 Ryugu was monitored during the proximity phase of Hayabusa2, no significant change in period was confirmed. To compare the results of observations and numerical simulations in terms of the YORP effect on Ryugu, we have to wait for the next opportunity of light curve acquisition.

Since the YORP modeling by Rubincam (2000), many numerical studies based on three-dimensional shapes of real asteroids have been performed. The computational models of the YORP effect have been developed to incorporate non-zero thermal conductivity (Čapek & Vokrouhlický, 2004) and projected shadows (Vokrouhlický & Čapek, 2002). The advanced thermophysical model (ATPM) proposed by Rozitis and Green (2011, 2012) completely implemented both the reabsorption of thermal emission due to uneven terrain and the surface roughness effect to deflect radiation in the direction of the Sun. Moreover, it has been found that lateral heat conduction is likely to significantly impact the thermal torque (Golubov et al., 2014; Ševeček et al., 2016), which has been neglected in most YORP models that solve the one-dimensional heat conduction problem. However, an all-in-one simulation method is computationally costly and difficult to apply to highly accurate shape models acquired by spacecrafts.

In this study, we aim to demonstrate the YORP-induced spin evolution of Ryugu and compare its time scale with the surface age of the asteroid. Although a simplified computational model is used herein (Section 2), we compared various types of Ryugu's shape models (Section 3) to overcome the inherent problem of numerical YORP modeling, in which the net torque is highly dependent on input shape models (Statler, 2009). In Section 4, we evaluate the model sensitivity to shape and compare our numerical model with another thermophysical model. In Section 5, we associate the spin alteration of Ryugu with geological events that have occurred on the asteroid.

Table 2. Notation in this paper.

Symbol	Description
A	Geometric albedo
s_i	Shadowing factor of the ith surface element (1 for shadow or 0 for insolation)
Φ	Solar irradiation per unit area on a body's orbit
$\hat{\boldsymbol{n}}_i$	Normal vector to the ith surface element
$\hat{\boldsymbol{r}}_{\boldsymbol{sun}}$	Direction of the Sun
ϵ	Emissivity of the body's surface
σ	Stefan-Boltzmann constant
T_i	Temperature of the ith surface element
K	Thermal conductivity of the material
$d\boldsymbol{f}_i$	Thermally induced force on the ith element
c	Speed of light
dS_i	Area of the ith element
$\boldsymbol{\tau}$	YORP torque on the body
$\boldsymbol{r}_i$	Centroid position of the ith element
N_{S}	Number of surface elements
$\boldsymbol{L}$	Angular momentum of rotation
C	Moment of inertia around the shortest axis
ω	Angular velocity of rotation
$\hat{\boldsymbol{s}}$	Direction of the spin pole
ε	Obliquity of the spin pole
ψ	Longitude of precession

2 Method of YORP Simulation

To calculate the thermally induced torque on an asteroid, we need to evaluate the surface temperature or radiation energy flux of the body's surface based on its orbit, spin state, and irregular shape. Subsequently, we simply have to integrate the equation of motion for the asteroid's rotation. All symbols used in this section are listed in Table 2.

2.1 Thermal model

We begin with the energy conservation law at each surface element of a small body's shape. The following equation presents the balance between the incident energy from sunlight (left-hand side) and the sum of energy derived from thermal re-radiation from the surface element and heat conduction into the ground (right-hand side).

$$(1 - A)(1 - s_i)\Phi(\hat{\boldsymbol{n}}_i \cdot \hat{\boldsymbol{r}}_{sun}) = \epsilon\sigma T_i^4 + K\hat{\boldsymbol{n}}_i \cdot \nabla T_i \tag{1}$$

In this study, we calculated the energy flux $\Phi(t)$ in each time step based on the Kepler motion of the asteroid around the Sun.

$$\Phi(t) = \Phi_{\mathrm{Earth}} \left(\frac{r_{\mathrm{Earth}}}{r_{\mathrm{body}}(t)} \right)^2 \tag{2}$$

The solar irradiation at the Earth's orbit $r_{\mathrm{Earth}} = 1$ AU is called the solar constant Φ_{Earth}, and it is inversely proportional to the square of the body's distance from the Sun. It greatly influences the strength or time scale of the YORP effect depending on the orbital semi-major axis. For example, there is a difference in the energy flux by a factor of approximately six between the near-Earth orbit (~ 1 AU) and inner main belt (~ 2.5 AU). Asteroid Ryugu exhibits seasonal variation in solar irradiation by a few times because of its eccentric orbit. We used 1366.0 W/m^2 for the solar constant in our simulations.

The left-hand side of Equation 1 expresses the amount of solar energy absorbed by the ith surface element of the shape model. Therefore, the factor $(\hat{\boldsymbol{n}}_i \cdot \hat{\boldsymbol{r}}_{sun})$ decreases the solar irradiation per unit area depending on the tilt of the element. On the night-side of the body, this factor becomes negative, and solar irradiation is supposedly turned off. In addition, we implemented a ray-trace algorithm to check whether each element is illuminated or not at a certain time, as implemented in, e.g., Breiter et al. (2009) and Rozitis and Green (2012). The shadowing factor, s_i, returns an integer of 1 or 0, depending on whether solar rays towards the ith element are blocked by other elements or not, respectively. To reduce the computation time, we sometimes ignore the shadowing effect in our later simulations and perform the so-called "pseudo-convex" model, originally implemented in Rubincam (2000).

The right-hand side of Equation 1 represents the energy released from each surface element, which includes the thermal radiation and heat flux of the body's interior. Some authors implemented one-dimensional thermophysical modeling to evaluate the surface temperature (e.g., Čapek & Vokrouhlický, 2004). This study simplified the computation of thermal radiation using the Rubincam (2000) approximation Rubincam (2000), which assumed

(1) zero-conductivity and (2) Lambert radiation from each surface element. According to assumption (1), we can neglect the conduction term in Equation 1 as follows:

$$(1-A)(1-s_i)\Phi(\hat{\boldsymbol{n}}_i \cdot \hat{\boldsymbol{r}}_{sun}) \approx \epsilon\sigma T_i^4 \tag{3}$$

This equation holds that the incident energy from sunlight is immediately emitted from the surface with no time lag. The second assumes that each surface element isotropically radiates energy, with the same intensity of infrared radiation observed from any angle. The Lambert radiation assumption results in a simple formula for the force exerted on each surface element (Rubincam, 2000; Vokrouhlický & Čapek, 2002):

$$d\boldsymbol{f}_i = -\frac{2}{3}\frac{\epsilon\sigma T^4}{c}\hat{\boldsymbol{n}}_i dS_i \tag{4}$$

$$= -\frac{2\Phi}{3c}(1-s_i)(\hat{\boldsymbol{n}}_i \cdot \hat{\boldsymbol{r}}_{sun})\hat{\boldsymbol{n}}_i dS_i \tag{5}$$

The thermal "kick-back" force, $d\boldsymbol{f}_i$, is directed opposite of the facet normal, $\hat{\boldsymbol{n}}_i$, and its magnitude is proportional to the area of the element dS_i. The thermal radiation, $\epsilon\sigma T^4$, can be replaced by the incident energy based on the assumption in Equation 3. We convert the factor $(1-A)$ to 1 to combine the effects of scattering on the surface. If the scattered light reflects isotropically, like thermal radiation, we can add its contribution to the factor $(1-A)$.

We can then compute the net torque, $\boldsymbol{\tau}$, of the YORP effect by integrating the above force over the entire surface of the asteroid. Given a polyhedral shape model covered with N_{S} triangular meshes, one simply has to sum the torque on every surface element as a cross product of the element's position, $\boldsymbol{r}_i$, and thermal kick-back, $d\boldsymbol{f}_i$, as follows:

$$\boldsymbol{\tau} = \int_S \boldsymbol{r} \times d\boldsymbol{f} = \sum_{i=1}^{N_{\mathrm{S}}} \boldsymbol{r}_i \times d\boldsymbol{f}_i \tag{6}$$

2.2 Equation of motion

Given uniform rotation around the shortest axis, the angular momentum $\boldsymbol{L}$ of a spinning body is simply expressed as follows:

$$\boldsymbol{L} = C\omega\hat{\boldsymbol{s}} \tag{7}$$

Here, the direction of $\boldsymbol{L}$ always matches that of the spin pole $\hat{\boldsymbol{s}}$ by neglecting small components of the angular velocity about the other axes. Contrarily to a typical YORP time scale ($\sim$ millions of years), the rotation pole is considered to be quickly relaxed to the shortest axis by energy dissipation associated with inelastic distortion (Efroimsky, 2001; Mysen, 2006). The YORP-induced torque, $\boldsymbol{\tau}$, in Equation 6 changes the angular momentum of the asteroid, and the equation of motion is expressed as follows:

$$\frac{d\boldsymbol{L}}{dt} = \boldsymbol{\tau} \tag{8}$$

Some authors decompose the above equation into three essential parameters to describe the spin state of the body. According to the expression given by Bottke et al. (2006), the equation of motion is expressed by time derivatives of angular velocity ω, obliquity ε, and longitude of precession ψ:

$$\frac{d\omega}{dt} = \frac{\tau_\omega}{C} \equiv \frac{\boldsymbol{\tau} \cdot \hat{\boldsymbol{s}}}{C} \tag{9}$$

$$\frac{d\varepsilon}{dt} = \frac{\tau_\varepsilon}{C\omega} \equiv \frac{\boldsymbol{\tau} \cdot \hat{\boldsymbol{e}}_{\perp 1}}{C\omega} \tag{10}$$

$$\frac{d\psi}{dt} = \frac{\tau_\psi}{C\omega} \equiv \frac{\boldsymbol{\tau} \cdot \hat{\boldsymbol{e}}_{\perp 2}}{C\omega} \tag{11}$$

The first term, τ_ω, is a component of the YORP toque parallel to the spin pole and changes the angular velocity of rotation or the period. The other two components, τ_ε and τ_ψ, are components along the basis vectors perpendicular to the pole, as shown in the following equations and Figure 1:

$$\hat{\boldsymbol{e}}_{\perp 1} \equiv \frac{(\hat{\boldsymbol{N}} \cdot \hat{\boldsymbol{s}})\hat{\boldsymbol{s}} - \hat{\boldsymbol{N}}}{\sin\varepsilon} \tag{12}$$

$$\hat{\boldsymbol{e}}_{\perp 2} \equiv \frac{\hat{\boldsymbol{s}} \times \hat{\boldsymbol{N}}}{\sin\varepsilon} \tag{13}$$

Thus, in Equations 10 and 11, the torque components τ_ε and τ_ψ change the obliquity of the spin pole and induce precession of rotation, respectively. The obliquity, ε, is defined as the axial tilt angle between the spin normal vector $\hat{\boldsymbol{s}}$ and a normal vector $\hat{\boldsymbol{N}}$ to the body's orbital plane. In fact, although the torque component along $\hat{\boldsymbol{e}}_{\perp 2}$ may excite wobbling rotation, we assume that the spin pole is quickly relaxed toward uniform rotation around the shortest axis by energy dissipation, and thus we focus on changes in ω and ε.

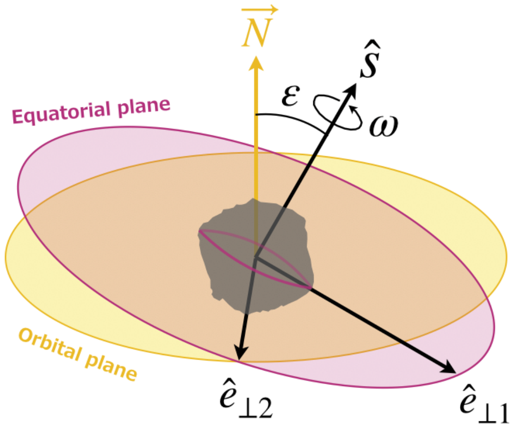

Figure 1. Basis vectors for a spinning body.

3 Results

3.1 Year-averaged torque on Ryugu

For the YORP modeling of asteroid Ryugu, we utilized the orbital elements, spin-pole orientation, and rotation period published by Watanabe et al. (2019) (see Table 1). As a nominal shape model for this study, we chose the 49152-mesh SPC model released on August 2, 2019. The mean mesh size of the shape model (i.e., mean diameter of circles of equivalent areas) was 8.4 m. Herein, we present the results of this nominal model and later compare the resultant YORP effects between shape models of different resolutions, release dates, and 3D reconstruction methods. We divided the cycle of Ryugu's rotation into 72 equal parts (every 5 degrees of the rotation angle) and computed the YORP torque, $\boldsymbol{\tau}$, at each time step. For a rotation period of 7.6 h, the interval of time steps was 382 s. The simulation was stopped when the asteroid completed one orbit (474 days; 107 288 time steps).

Figure 2 illustrates the time variations of each torque component over the cycles of Ryugu's rotation (left panels) and revolution (right panels). As the torque variation is not completely cancelled over the cycles because of Ryugu's irregular shape, the residual induces a secular change in the spin parameters. A net torque, $\bar{\boldsymbol{\tau}}$, can be obtained by averaging the diurnal and seasonal variations. In the nominal case of the SPC-based 49k-mesh model with the self-shadowing effect, the year-averaged torque results in $(\bar{\tau}_\omega, \bar{\tau}_\varepsilon, \bar{\tau}_\psi) = (-0.161, 0.161, 4.05)$ N $\cdot$ m. The negative value of the ω-related component implies that the angular velocity of Ryugu is currently decreasing. According to Equation 9 and the

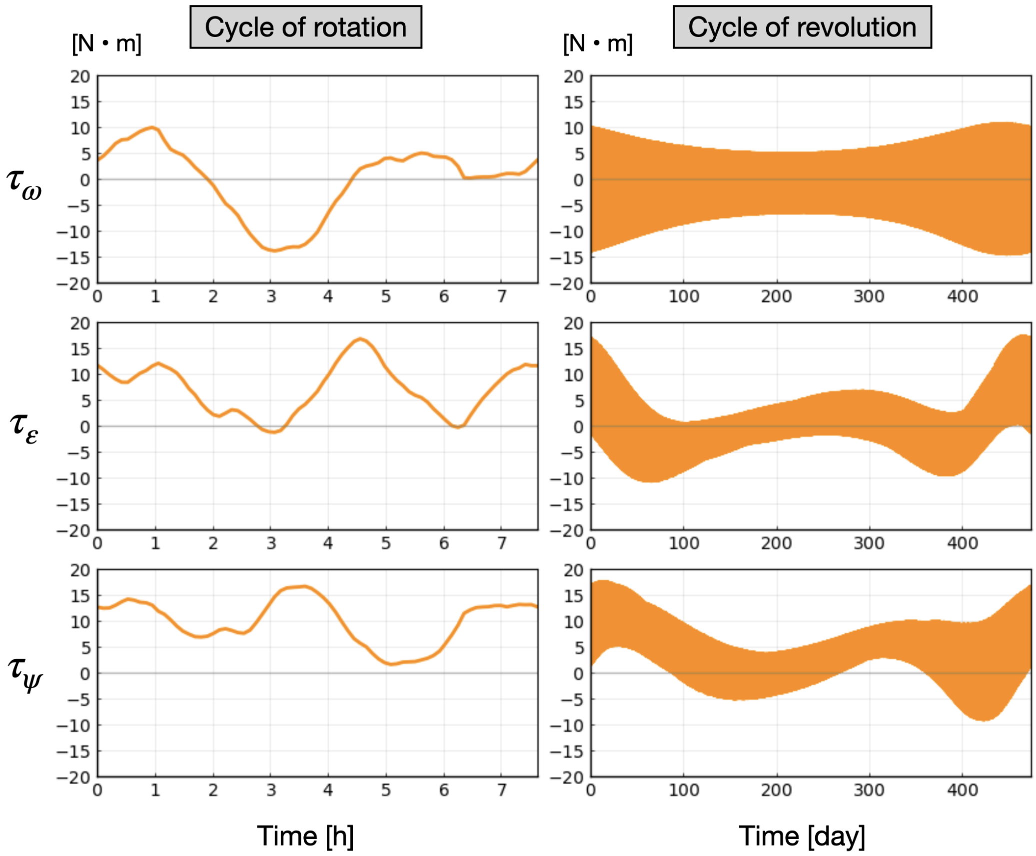

Figure 2. Diurnal and seasonal variations of YORP torque components.

moment of inertia of 4.04×10^{16} kg $\cdot$ m^2, the change in the spin rate of Ryugu corresponds to $\dot{\omega} = -1.71 \times 10^{-6}$ deg/day^2. The strength of the YORP effect is often characterized by the YORP time scale (Rubincam, 2000), which corresponds to the time required to double or halve the angular velocity ω. For Ryugu, the YORP time scale for doubling the current rotation period corresponds to $t_{7.6\mathrm{h} \to 15.2\mathrm{h}} = 0.909$ million years. Note that this time scale is computed assuming that the rotation decelerates at a constant rate. To investigate the detailed process of spin evolution and its time scale, the reorientation of the spin axis must be considered.

In addition, the resultant rate of deceleration may vary depending on the meter-scaled differences of an input shape model (Statler, 2009). Although the highest-resolution models described in Watanabe et al. (2019) are well matched regardless of the two different techniques of reconstruction, they may contain artifacts in the polar region where fewer images are obtained, and/or there are slight differences when reducing the resolution of the shape models. Therefore, we surveyed various versions of shape models to determine the sensitivity of the input model. Table 3 lists the year-averaged torque on each shape model considering the self-shadowing effect. A shape model ID consists of the reconstruction technique (SFM or SPC), number of surface meshes, and release date (in YYYYMMDD format). The YORP simulations are performed only for the low-resolution models of ∼49k meshes because detection of locally generated shadows at every time step is computationally expensive. In all cases, the net torque yields a negative rate of change for angular velocity ω and a positive one for obliquity ε, indicating that Ryugu is currently spinning down and increasing its obliquity toward 180°. The torque component that causes precession is difficult to cancel during a cycle of revolution and yields greater net torque. The deceleration of Ryugu's rotation is consistent with its fast rotation in the past. The spin-down time scales are estimated assuming that the spin rate has been decreasing at a constant rate from a 3.5-h to a 7.633-h period. The estimated time scales of deceleration vary from 0.58 to 8.7 million years. The cases can be classified into two types: type II, which yields more rapid deceleration ($t_{3.5\mathrm{h}\to7.6\mathrm{h}} < 1$ Myr), and type IV, which yields slower deceleration (predominantly $t_{3.5\mathrm{h}\to7.6\mathrm{h}} > 1$ Myr). The classification criteria are detailed in Section 3.2.

3.2 Obliquity dependence of YORP

The spin rate ω and obliquity ε are essential parameters for simulating the long-term evolution of a rotating body. As the spin-pole direction and obliquity change, the solar irradiation conditions of the body vary. In this section, we demonstrate the dependence of the YORP effect on obliquity and predict Ryugu's spin evolution in millions of years. To achieve this, we calculate the thermal net torque on the asteroid, as in the previous section, but for various obliquities from 0° to 180°. Figure 3 shows the rates of change in ω (dashed) and ε (solid) as functions of ε, as derived from the nominal model (SHAPE_SPC_49k_v20190802) in a similar manner to previous studies (Rubincam, 2000; Vokrouhlický & Čapek, 2002; Čapek & Vokrouhlický, 2004; Bottke et al., 2006). It should be noted that the solid curve τ_ε/C $(= \omega\dot{\varepsilon})$ has three "asymptotic" nodes at $\varepsilon = 0°$, $90°$, and $180°$. The thermal torque tends asymptotically toward one of these nodes depending on the initial obliquity ε_0. For the nominal shape model, the boundaries at $\varepsilon = 37°$ and $143°$ dominate the destiny of the spin evolution and whether the spin pole finally stands upright ($\varepsilon \to 0°$ or $180°$) or falls on the orbital plane ($\varepsilon \to 90°$). On the other hand, the dashed curve τ_ω/C $(= \dot{\omega})$ in Figure 3 shows that the rotation of Ryugu decelerates at every obliquity. In this case, Ryugu should

Table 3. Thermal net torque and deceleration time scales derived from different shape models. According to Equations 9 to 11, the torque components divided based on the moment of inertia are shown as $\dot{\omega} = \tau_\omega / C$, $\omega\dot{\varepsilon} = \tau_\varepsilon / C$, and $\omega\dot{\psi} = \tau_\psi / C$. The self-shadowing effect is considered.

Model ID SHAPE_ ...	$\dot{\omega}$	$\omega\dot{\varepsilon}$ $\times 10^{-6}$ [deg/day^2]	$\omega\dot{\psi}$	$t_{3.5\mathrm{h}\to 7.6\mathrm{h}}$ [Myr]	Classification
SFM_49k_v20180705	−5.207	2.282	38.34	0.7032	II
SFM_49k_v20180714	−5.834	2.523	39.82	0.6277	II
SFM_47k_v20190130	−6.261	2.691	43.28	0.5849	II
SPC_49k_v20180705	−5.065	3.410	46.07	0.7230	II
SPC_49k_v20180710	−5.010	2.973	43.03	0.7310	II
SPC_49k_v20180717	−4.781	2.785	40.81	0.7660	II
SPC_49k_v20180719_2	−3.647	2.367	39.12	1.004	II
SFM_49k_v20180725_2	−4.560	1.775	40.38	0.8030	IV
SFM_49k_v20180804	−3.531	1.667	39.73	1.037	IV
SPC_49k_v20180731	−0.5352	1.561	41.35	6.842	IV
SPC_49k_v20180810	−0.6878	1.434	39.71	5.324	IV
SPC_49k_v20180816	−0.4212	1.362	39.81	8.693	IV
SPC_49k_v20180829	−0.6152	1.586	42.25	5.952	IV
SPC_49k_v20181014	−1.706	1.735	43.17	2.147	IV
SPC_49k_v20181109	−1.368	1.719	43.03	2.676	IV
SPC_49k_v20181204	−0.6796	1.477	42.91	5.388	IV
SPC_49k_v20190308	−1.207	1.607	43.35	3.035	IV
SPC_49k_v20190328	−1.069	1.548	42.99	3.426	IV
SPC_49k_v20190802*	−1.705	1.701	42.86	2.148	IV
SPC_49k_v20200323	−1.406	1.245	42.22	2.604	IV

*Nominal shape model in this study

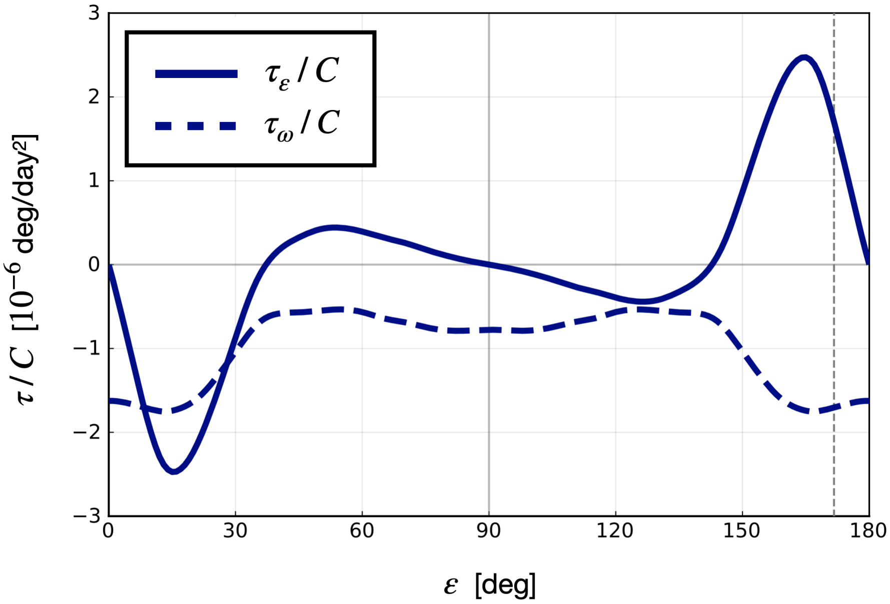

Figure 3. Obliquity dependence of the thermal torque derived from the nominal shape model. The self-shadowing effect is considered. Rates of change in obliquity ε (solid) and spin rate ω (dashed) as functions of the obliquity. The vertical dashed line at $\varepsilon = 171.6°$ represents the nominal obliquity observed by Hayabusa2.

reach a permanent spin-down phase at one of the three asymptotic obliquities. The vertical dashed line in Figure 3 represents the current obliquity of Ryugu ($\varepsilon = 171.64°$), which was observed by Hayabusa2 (Watanabe et al., 2019). As already mentioned in 3.1, Ryugu is currently considered to be spinning down with the obliquity of the spin pole increasing toward 180°. In contrast, the spin of asteroid 101955 Bennu (a target body of NASA's OSIRIS-REx mission) is accelerating with an obliquity of nearly 180° (Nolan et al., 2019; Hergenrother et al., 2019).

Vokrouhlický and Čapek (2002) performed YORP simulations using randomly generated shapes of virtual asteroids and classified hundreds of the cases according to the obliquity they would settle into after sufficient time. For types I and II, the spin axes will eventually fall ($\varepsilon \to 90°$) and rise ($\varepsilon \to 0°$ or 180°), respectively. These two types account for 80% of the 500 cases. A further 10% of the cases are classified as type III, which have different asymptotic obliquities from the above two types (e.g., $\varepsilon = 30°$ and 150° in the shape of asteroid 2063 Bacchus). Type IV is the remaining minority, which has three asymptotic obliquities at $\varepsilon = 0°$, $90°$, and $180°$ depending on the initial obliquity. The nominal case plotted in Figure 3 is classified as this type.

Next, we examine the ε-dependence of the net torque on the various shape models in Table 3. The self-shadowing effect is considered in this survey. It is found that the YORP effect on Ryugu results in either type II or IV. The seven cases in type II and 13 cases in type IV are shown separately in Figure 4. Considering the symmetry of the even/odd functions, half of each is omitted from display. The rates of change in the spin rate on the left and obliquity on the right can be observed. In the high-obliquity area around the nominal obliquity ($\varepsilon = 171.6°$; marked by the gray dashed line), both types tend toward the state of the upright spin pole. If Ryugu follows type IV evolution, it is necessary for the body to start with an obliquity of over $\sim 140°$ to reach the current value. Otherwise, Ryugu's spin axis will become parallel to the orbital plane. When the axis of rotation becomes upright (at an obliquity of $0°$, equivalent to $180°$), type II shapes tend to yield greater deceleration than type IV shapes. Thus far, the time scale of deceleration depends on subtle differences in the shape models to be entered and the indeterminacy of approximation in our numerical model, but Ryugu is likely to be spinning down with the pole rising toward $\varepsilon = 180°$. Changes in Ryugu's spin state over time based on the obliquity dependence is discussed in Section 5.1.

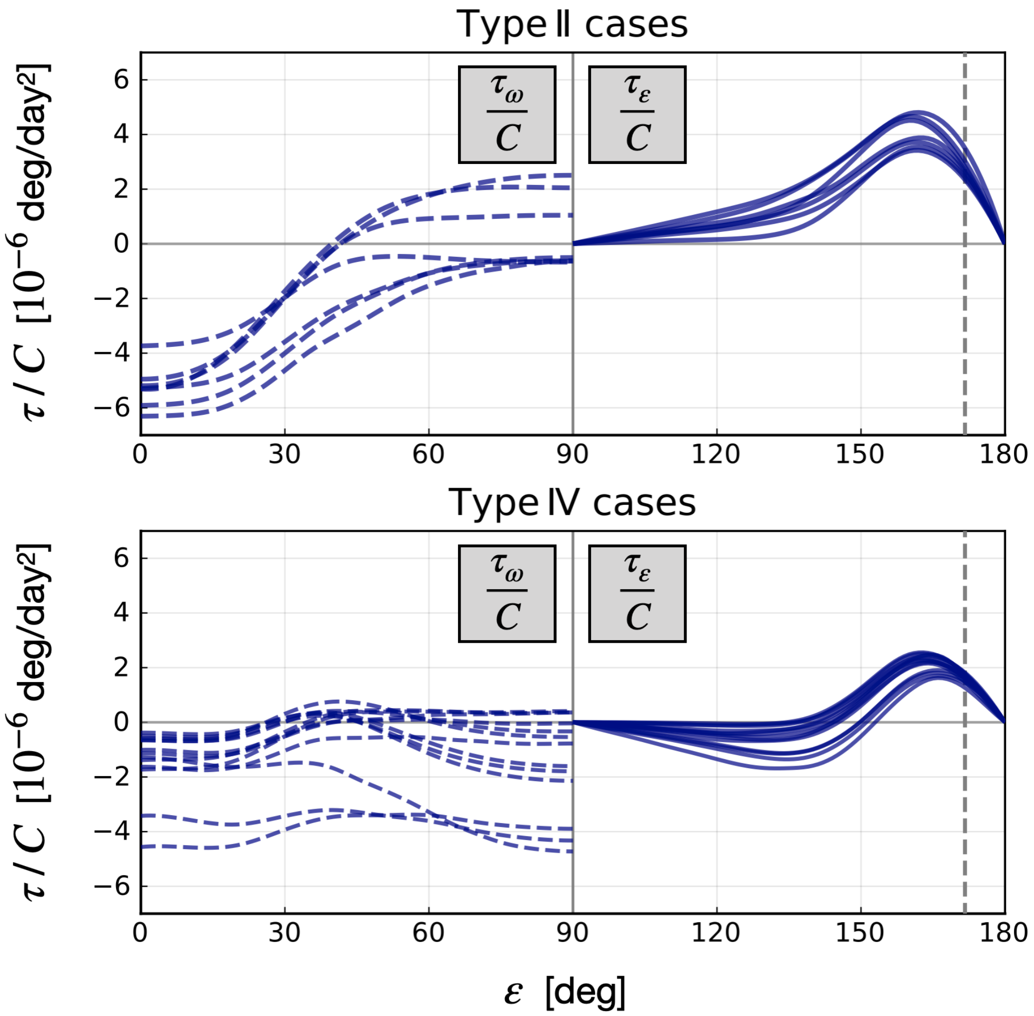

Figure 4. Obliquity dependence surveyed for 20 shape models in Table 3. The self-shadowing effect is considered. The left half of each panel shows the thermal torque component required to change the spin rate as a function of obliquity. The right half shows the torque component required to change the obliquity. The 20 models are classified into types II (seven cases in the upper panel) and IV (13 cases in the lower panel) according to Vokrouhlický's criteria.

4 Validity of YORP Simulations

In general, a numerical simulation of the YORP effect strongly depends on small-scale topographic features of the shape model (Statler, 2009; Breiter et al., 2009). To evaluate this uncertainty, we prepared "perturbed" shape models from the nominal model used in Section 3 and repeated the YORP simulations (following the numerical experiments by Nolan et al. (2019)). The perturbed models were created by applying noise to the nominal model on a scale similar to the facet size. Each vertex of the original shape model was randomly shifted in the radial direction, for example, within a range of ± 1 m. We demonstrated 1000 perturbed models for each noise of ± 1 m and ± 2 m by ignoring the self-shadowing effect. The upper panels in Figure 5 illustrate the nominal shape model and perturbed models with different noise levels. The mean mesh size $\bar{D}_{\mathrm{S}}$ of the nominal shape model is 8.4 m, which is hereby defined as the mean diameter of circles of equivalent areas. As the noise increases, more artificial bumps appear on the surface. The histograms show the distributions of the rates of year-averaged acceleration, $\dot{\omega}$. Given the noise within ± 1 m (orange), $\dot{\omega}$ is distributed around the nominal value of -1.32×10^{-6} [rad/day^2] with a 1σ uncertainty of $\pm 19\%$. For larger-scale noise in the shape model, the distribution of the YORP acceleration spreads, and some of the cases change to spinning up ($\dot{\omega} > 0$). According to Watanabe et al. (2019), the shape models of 3 million meshes derived from SPC and SfM are well matched within a standard deviation of elevation of ~ 1.5 m. The lower-resolution model used in this study was created by downsizing the 3M-mesh model. Random artifacts on the shape model at the meter scale affect the magnitude of the resultant YORP effect to some extent; however, they are unlikely to change the sign of the acceleration rate.

We also provide an overview of the YORP acceleration dependence on the resolution of an input shape model in the case of Ryugu. Ignoring the self-shadowing effect, we performed YORP simulations up to the highest-resolution models. The SPC-based models of each version have four different resolutions (i.e., numbers of surface facets): $N_{\mathrm{S}} = 49\ 152$, 196 608, 786 432, and 3 145 728. The SfM models are also released with approximately the same resolutions. Figure 6 represents the YORP acceleration rates derived from the various shape models as functions of their resolutions. The SPC and SfM models are plotted as blue circles and orange triangles, respectively. Shape models released on the same date are connected with each other. A lower-resolution model was created by reducing the highest-resolution model released on the same date. Except for the five shape families (the SPC models released on 2018-07-31, 2018-08-10, 2018-08-16, 2018-08-29, and 2020-03-23), the

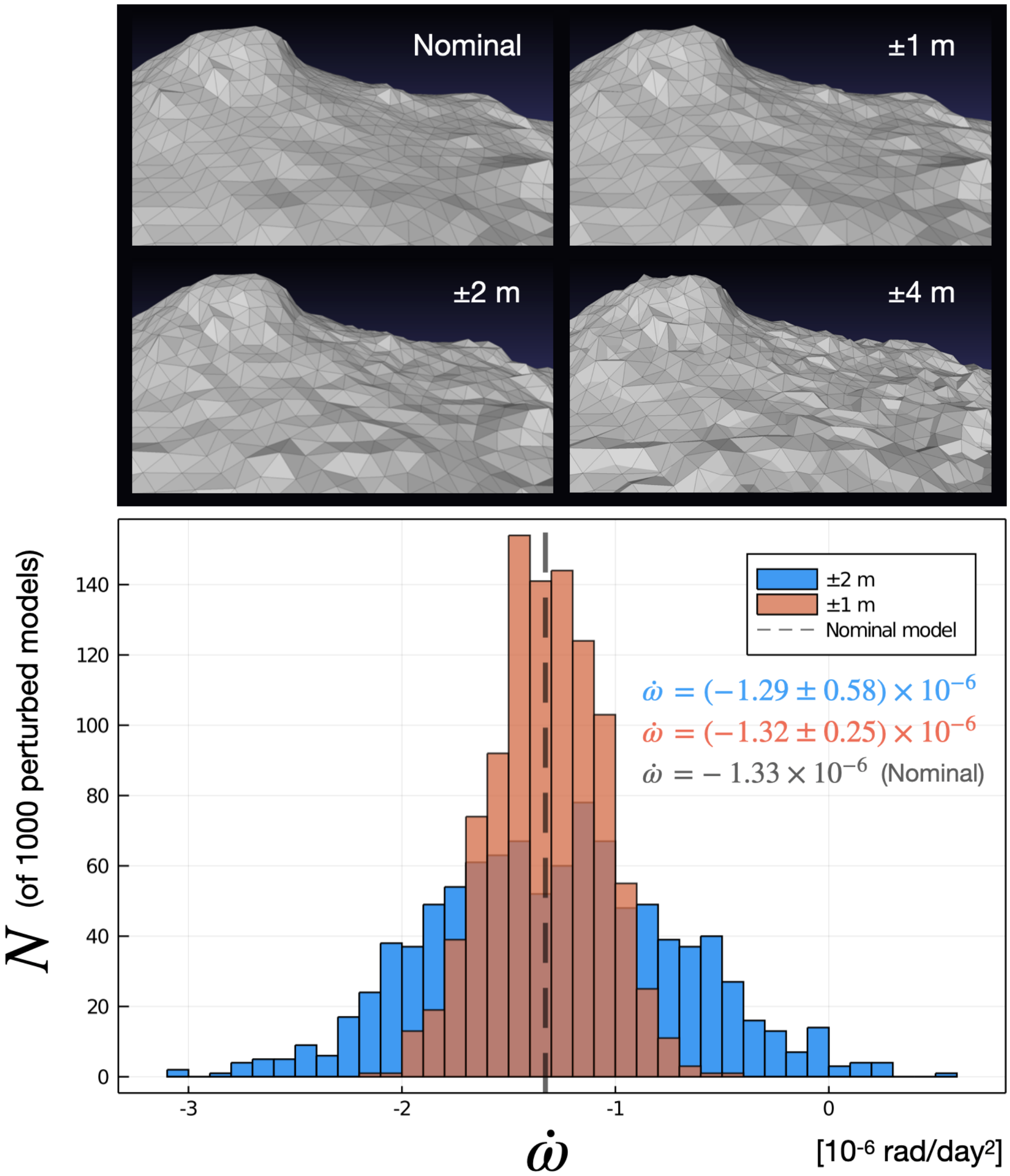

Figure 5. YORP acceleration/deceleration derived from perturbed shape models. The self-shadowing effect is neglected in this survey.

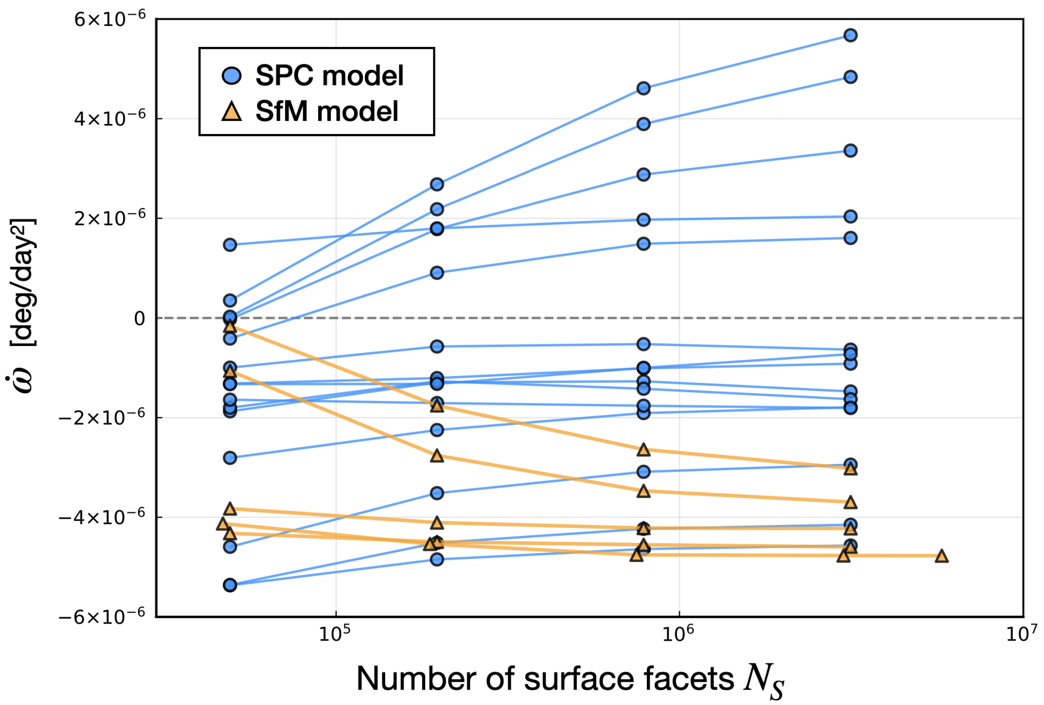

Figure 6. Rotational acceleration as a function of the resolution of the input shape models. The self-shadowing effect is neglected.

remaining models yielded negative rates of rotational acceleration. In the low-resolution models of $\sim$ 49k meshes, however, we confirmed that all cases resulted in deceleration of rotation when considering the self-shadowing effect (see Table 3). As reported by Breiter et al. (2009), some shape families tend to yield greater rates of acceleration/deceleration as the resolution of the shape models increases without converging to a certain value. The higher resolution model has a larger variance in the slopes of the surface facets, and the magnitude of the resultant acceleration can increase. A detailed thermal model, as described below, is computationally costly, and its convergence to the resolution of the shape model has not yet been confirmed.

In this study, we approximated the balance of incoming and outgoing radiation using a simple model based on Rubincam (2000). We examined the extent to which this model works for the YORP simulation on asteroid Ryugu. Rugged topography can block direct sunlight and cast a shadow on the surface. This self-shadowing effect could generate a significant bias in the radiation emitted from the body (Breiter et al., 2009). Herein, we turned self-shadowing on and off depending on the computation time. In addition, reabsorption of thermal emission from the surrounding ground ("self-heating") and nonzero thermal conductivity could alter the thermal torque exerted on the asteroid (Čapek & Vokrouhlický, 2004). A thermophysical model (TPM) was developed for simulating the distribution of the surface temperature on Ryugu and comparing its results with mid-infrared images obtained from the thermal infrared imager (TIR) on the Hayabusa2 spacecraft (Takita et al., 2017). We performed the TPM simulation using Ryugu's ephemeris and obtained the net torque component required to change the spin rate of Ryugu on August 1, 2018. The 200k-mesh SfM model (SHAPE_SFM_200k_v20180804) and a constant thermal inertia of $300\ \mathrm{J \cdot m^{-2} \cdot K^{-1} \cdot s^{-0.5}}$ (tiu) were used for the simulation. Figure 7 compares the diurnal variation of the thermal torque obtained for different thermal models. The blue curve in the lower panel considers the total irradiation energy accounting for the self-shadowing and self-heating effects (upper left panel), but zero conductivity is assumed in accordance with Equation 3. The orange curve represents the time variation of the thermal torque based on the distribution of surface temperature considering nonzero conductivity (upper right panel). The TPM simulation solves the one-dimensional heat conduction equation in the depth direction on each facet with the surface boundary condition according to Equation 1. The gray dashed curve is derived from our implementation of Rubincam's model with the spin phase fitted to the TPM simulation.

The blue curve indicates that the local shadows on the surface generate a fine irregularity in the time variation in the thermal torque. By averaging its ω-related component, the shadowing effect is shown to increase the magnitude of the YORP deceleration compared to the simplest model in this period of time. The daily averaged torque was (1) $\bar{\tau}_\omega = -0.365$ $\mathrm{N \cdot m}$ in Rubincam's model and (2) $\bar{\tau}_\omega = -0.407\ \mathrm{N \cdot m}$ in the shadowing model. In one revolution cycle, we confirmed that the shadows increased or decreased the magnitude of deceleration randomly. As shown by the orange curve, thermal inertia lowered the contrast of radiation between the hemispheres of daytime and nighttime and lowered the peak of the thermal torque. In addition, a phase delay of approximately 15 min can be observed between the nonzero conductivity model and the others. Nonzero conductivity, however, does not change the total amount of radiation throughout one rotational cycle. Therefore, the phase lag of the thermal torque variation was insignificant to the net acceleration or deceleration, as established previously (Čapek & Vokrouhlický, 2004). On the other hand, the delayed radiation due to thermal inertia is considered to be more effective in altering the spin pole direction (Čapek & Vokrouhlický, 2004; Breiter et al., 2007; Mysen, 2008;

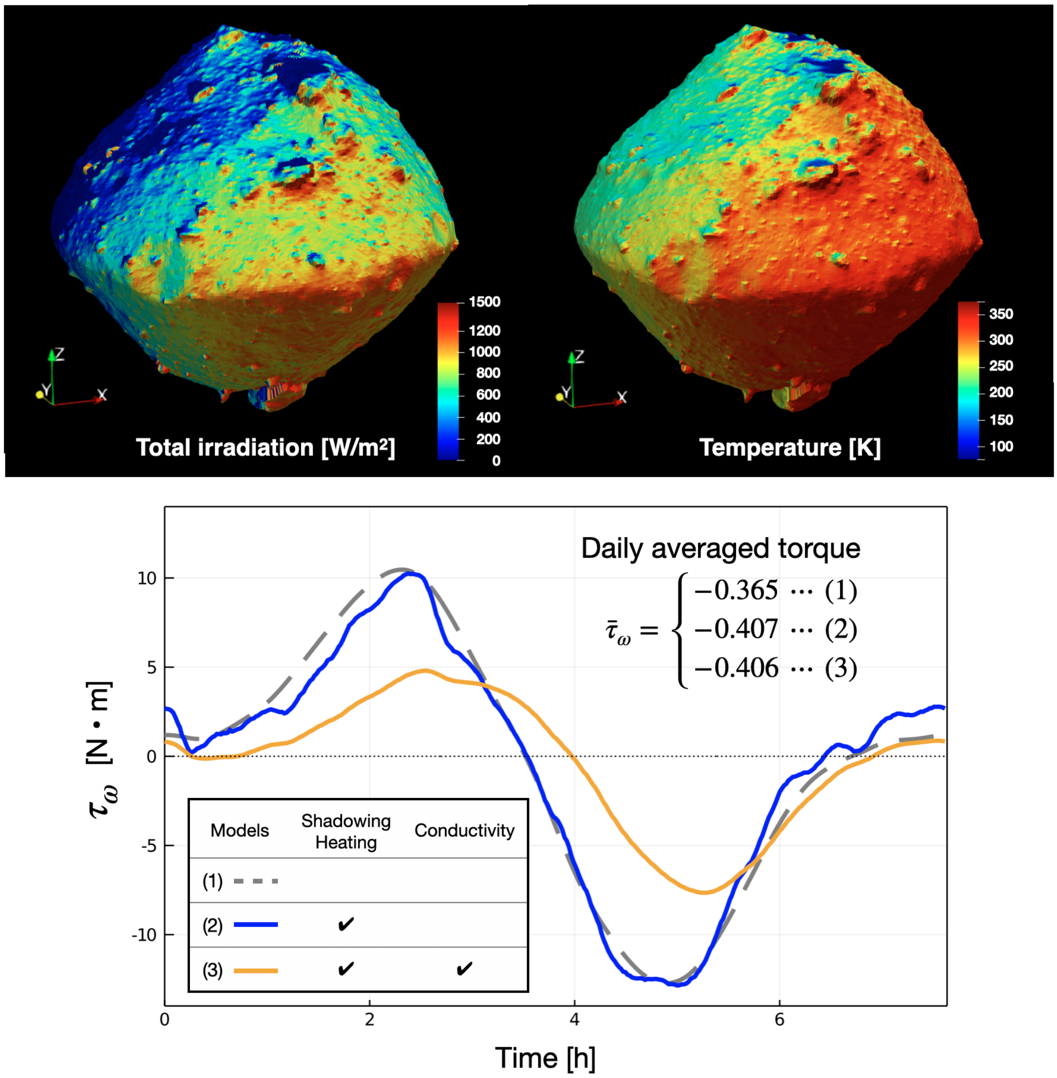

Figure 7. (*Upper*) Spatial distribution of the total radiation input to each facet and the surface temperature obtained using the TPM (Takita et al., 2017). (*Lower*) Time variation of the thermal torque component required to change the spin rate of Ryugu over a diurnal cycle. The blue curve considers the self-shadowing and self-heating effects in addition to our implementation of Rubincam's model (gray curve). Thermal inertia ($\Gamma = 300$ tiu) is also accounted for in the orange curve.

Scheeres, 2007). As revealed by the infrared observations of TIR and the Mobile Asteroid Surface Scout (MASCOT) lander, the thermal inertia of Ryugu's surface material was estimated as approximately 300 tiu (Okada et al., 2020) or 225 ± 45 tiu (Shimaki et al., 2020), corresponding to a thermal conductivity of ~ 0.1 W/(m $\cdot$ K) (Grott et al., 2019). Although Ryugu is spinning at a relatively mild spin rate and is covered with porous boulders of low conductivity, the dependence of the net torque on thermal inertia should be investigated in the future.

5 Discussion

5.1 YORP-induced spin evolution of Ryugu

We explored the effect of the obliquity of Ryugu's spin pole on the thermally induced torque in Section 3.2. This enables us to predict the long-term evolution of the spin state over millions of years. The top panels in Figure 8 demonstrate representative examples of the ε-dependence of the YORP effect for type II and IV cases. The latest SFM model (SHAPE_SFM_47k_v20190130) and our nominal model (SHAPE_SPC_49k_v20190802) were chosen from each group. Again, the self-shadowing effect was considered, and the current orbit of Ryugu was used ($a = 1.19$ AU). The middle and bottom panels represent the rotation period and obliquity of the asteroid, respectively, as functions of time after providing initial conditions. The initial rotation period is set to 3.5 h, obliquities range from 100° to 170°. The evolution paths follow the ε-dependence on the corresponding upper panels and the equations of motion in Equations 9 and 10. The currently observed spin parameters of Ryugu are marked at $P = 7.632$ h and $\varepsilon = 171.6°$ by gray dashed lines in each panel. The nominal case of type IV clearly shows that an initial obliquity smaller than 143° cannot achieve an upright spin pole. For the type II example, an upright spin pole can be achieved for any initial obliquity exceeding 90°. The time scale for the spin axis to rise ($\varepsilon \to 180°$) is within a few million years for the nominal case. For a type II case starting with a smaller obliquity, the spin pole can take nearly 5 million years to rise.

Moreover, we also surveyed for various initial rotation periods. The contour plots in Figure 9 show the time required for the rotation period to reach 7.632 h as a function of the initial obliquity and period. The same shape models as Figure 8 were used. In the nominal case of type IV, the time scale of rotational deceleration is within a few million years. Note that the possible obliquity must equal or exceed 143° to prevent the spin pole from collapsing onto the orbital plane. For the type II case, the spin-down time scale could be up to 6.5 million years if the body enters a collapsed spin-pole state with a small deceleration rate. Although the time scale varies depending on the input shape models, the path of the spin evolution is as described above.

As mentioned above, the YORP-induced torque is responsible for keeping the spin pole perpendicular to the orbital plane. However, the current obliquity of Ryugu is 172°, and it does not perfectly match 180°. Considering the relatively short time scale of change in the spin-pole direction, Ryugu is likely to have experienced a spin-related disturbance event

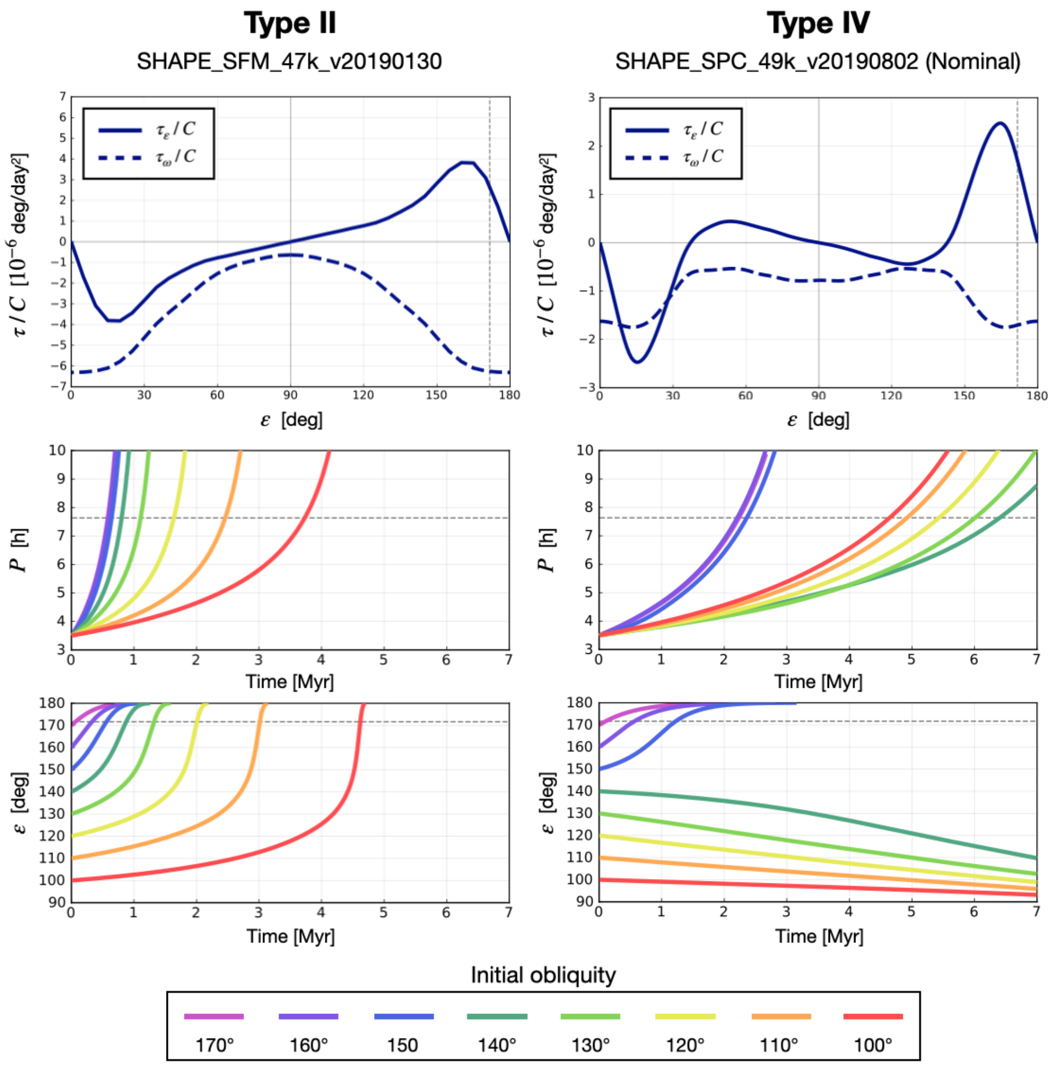

Figure 8. Paths of spin evolution according to representative examples of obliquity dependence on the YORP effect for type II (left) and type IV (right) cases. The top panels show the dependence of the thermal torque on obliquity. The middle and bottom panels plot the temporal evolution of the rotation period P and obliquity ε, respectively, assuming an initial period of 3.5 h and obliquities in the range of 100° – 170°. The horizontal gray dashed lines indicate the current period and obliquity of Ryugu.

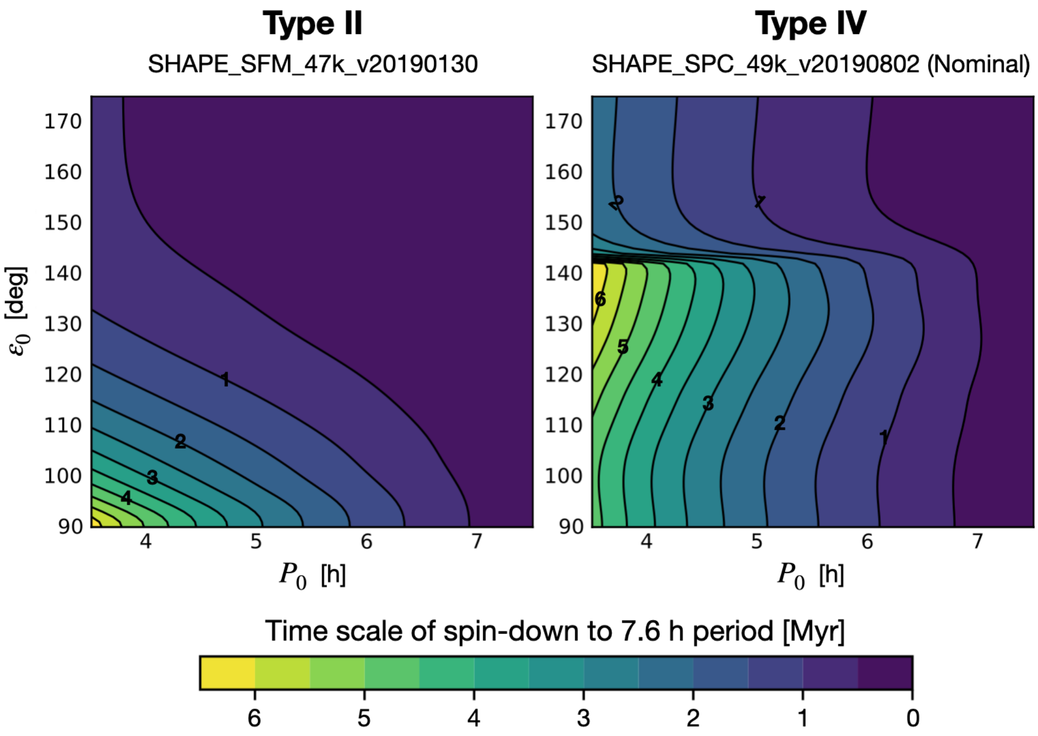

Figure 9. Time required to decelerate to the current rotation period of Ryugu as a function of the initial obliquity, ε_0, and period, P_0 for a type II (left) and type IV evolution (right).

within the last several million years. As a single event, a close encounter with a planet could potentially alter radically the angular momentum of a near-Earth asteroid (Scheeres et al., 2000; Benson et al., 2019). The spin modification due to the gravitational torque of a planet strongly depends on the hyperbolic orbit and spin-pole direction of the asteroid with respect to the planet. The kinetic energy of an impactor could also directly alter the angular momentum of an asteroid. The effect of an impact event on Ryugu is estimated in Section 5.2. A topographic change caused by crater formation could have altered the YORP effect on the body over its geological time scale. According to the list of craters on Ryugu compiled by Noguchi et al. (2021), the total area of all these craters is 3.65×10^5 m^2, which corresponds to approximately 13% of the total surface area of the body. In addition, prediction of non-uniform rotation is left for future work because the thermal torque can cause precession of the spin pole.

5.2 Effect of an impact event

The Hayabusa2 mission conducted an artificial cratering experiment using a small carry-on impactor (SCI), which revealed that the artificial crater on Ryugu was formed in the gravity-dominated regime owing to the significantly small cohesion of its surface materials (Arakawa et al., 2020). According to the conventional scaling law in this regime and other parameters from the impact conditions of the SCI experiment, Arakawa et al. (2020) provided the scaling law for the cohesionless surface of Ryugu as follows:

$$\pi_{\mathrm{R}} = 0.62 \times \pi_2^{-0.17} \pi_4^{0.0014} \tag{14}$$

where π_{R}, π_2, and π_4 are the conventional dimensionless parameters (Housen & Holsapple, 2011). Using this scaling law and the size of the largest crater observed on Ryugu, the maximum change in the rotation parameters owing to an impact can be estimated. The largest crater, *Urashima*, is 246.9 ± 7.0 m in diameter and is located near the equator (Noguchi et al., 2021). The other collision parameters are listed in Table 4. Therefore, we considered a chondritic meteorite of radius ~ 1 m that collided with a rotating spherical body similar to Ryugu at the mean impact velocity in the main belt. Assuming that the target body acquired all the kinetic energy of the impactor without any loss, the maximum change in the angular momentum was calculated to be $\Delta L = 4.1 \times 10^{10}$ kg $\cdot$ m^2/s when the impactor collided in a tangential direction to the spherical target. This increase is less than 1% of the original angular momentum of Ryugu, $L = 9.2 \times 10^{12}$ kg $\cdot$ m^2/s. Even if the impactor collided in the east–west direction at the equator, the change in the rotation period would be limited to approximately 120 s in both the acceleration and deceleration cases. In the event of a north–south collision, the direction of the spin pole would change by a maximum of only 0.25°. In reality, the change would be significantly smaller because of energy dissipation, etc. It can be concluded that even the formation of the largest crater on Ryugu would not have been able to disturb its rotation to such an extent.

5.3 Implications for geologic history of Ryugu

Despite the uncertainty in the numerical YORP modeling, this study strongly suggests that the YORP effect could have been a major factor in the rotational deceleration of Ryugu since its currently observed shape was formed. Our YORP simulation based on Ryugu's shape model yielded rates of change in angular velocity of $(-0.42 - -6.3) \times 10^{-6}$ deg/day^2 (see Table 3). In most cases, the spin pole of Ryugu was maintained for obliquities of nearly

Table 4. Impact parameters used to estimate the maximum change in the rotation of Ryugu.

Parameters	Notation	Value	Unit
Radius of *Urashima* crater	R	123	m
Impact velocity*	u	5300	m/s
Target density	ρ	1190	kg/m^3
Target gravity**	g	1.2×10^{-4}	m/s^2
Projectile radius	a	1.07	m
Projectile density	δ	3000	kg/m^3

*Equal to mean impact velocity in the main belt (Bottke et al., 1994).
**Corresponding to a spherical body with a GM of 30 m^3/s^2 and an equatorial radius of 502 m (Watanabe et al., 2019).

180°. In this obliquity range, the deceleration rate can be considered to be approximately constant in all cases (see the left side of Figure 4). Assuming a constant deceleration at these rates, it would have taken 0.58 – 8.7 million years to alter the rotation period from 3.5 to 7.6 h. This is consistent with the time scales (0.3–8.1 Ma) of spin deceleration estimated by Morota et al. (2020) based on crater counting, as previously discussed in Section 1.1.

As the YORP effect depends on the body's shape, the deceleration time scale corresponds to the time that has passed since the occurrence of a major change in topography during the fast rotation phase. Statistical analysis of fresher craters with bluer spectra on Ryugu indicated that the asteroid experienced surface reddening due to solar heating when it migrated from the inner main belt to the near-Earth orbit 0.3–8 million years ago (Morota et al., 2020). Hence, our estimated time scale of the rotational deceleration is comparable to the time that Ryugu has spent in the near-Earth orbit. A recent paper by Cho et al. (2021) estimated the surface age of each geological unit on the asteroid. According to these crater statistics, the equatorial ridge is the oldest terrain on Ryugu, thought to have formed 23 – 30 million years ago. This early deformation is consistent with the direct formation of the top shape during the accumulation of the rubble pile (Michel et al., 2020). However, the YORP deceleration time scale is much shorter than the formation age of the equatorial ridge. Therefore, a more recent resurfacing event may have impacted the YORP effect on Ryugu, becoming a tipping point in its dynamical history in terms of spin. A corresponding geological event could be the formation of the largest crater, *Urashima*, or the formation of the western bulge, which is considered to be a younger unit with fewer craters than the eastern hemisphere (Hirata et al., 2020). The formation ages of these units are estimated to be 5 – 12 and 2 – 9 Ma, respectively, depending on the timing of the orbital migration of Ryugu from the main belt to its near-Earth orbit (Cho et al., 2021). Our estimate of the deceleration time scale is comparable with the ages of these events, and it is possible that Ryugu had been spinning at a fast rate until the event time.

During fast rotation at a period of ~ 3.6 h, the Coriolis force may accumulate impact ejecta asymmetrically on a spinning body (Hirata et al., 2021). Some of the major craters in the equatorial region (e.g., *Urashima*, *Cendrillon*, and *Kolobok*) have higher rims on the west sides. These east-west asymmetric craters may bias the YORP effect on Ryugu. In the future, we need to consider the possibility that the formation of multiple craters has gradually altered the spin history of the body, or that the inward orbital migration decreased the heliocentric distance and hastened the spin alteration. In addition, roughness smaller than the size of the meshes (centimeter to decimeter) may have contributed to the increase in spin rate caused by thermal torque, known as the tangential YORP effect (Golubov & Krugly, 2012; Golubov et al., 2014; Golubov, 2017). The boulder-rich surface of Ryugu tends to impede rotational deceleration caused by the normal YORP and extend the time scale of the spin-down. As observed by the TIR on Hayabusa2, the surface roughness induces thermal infrared beaming toward the Sun (Okada et al., 2020), which also could dampen the magnitude of the YORP effect (Rozitis & Green, 2011, 2012).

The YORP simulation in this study also predicts the change in the direction of Ryugu's rotation axis. The currently observed shape of Ryugu yields the stability of the spin pole at an obliquity of 180°. For Ryugu, it is likely that the spin pole has remained perpendicular to the orbital plane even if a spin disturbance event has occurred, as explained in Section 5.1. In addition to the mass-shedding process on the surface of Ryugu, the pole stability may contribute to the formation of the latitudinal pattern in the visible and near-infrared spectra (Sugita et al., 2019). This may have protected the polar regions from sunlight and maintained their bluer spectra (Tatsumi et al., in prep.).

6 Conclusion

In this study, we investigated the YORP-induced spin evolution of asteroid Ryugu. We also confirmed that a simplified thermal model assuming zero thermal conductivity can compute the YORP torque exerted on Ryugu with sufficient accuracy. The approximation reduced the computational time and allowed us to examine various versions of the shape models. Regardless of the differences between the 3D construction methods and input image datasets, it is suggested that Ryugu is currently spinning down at a rate of (-0.42 – -6.3) $\times 10^{-6}$ deg/day^2, and a reasonable time scale of 0.58 – 8.7 million years is given for the spin alteration that has occurred since the fast rotation in the past. Combined with Hayabusa2 remote sensing data, our findings on the dynamical and geological history of Ryugu will contribute to the interpretation of future analyses of samples returning to Earth at the end of 2020.

Acknowledgments

We would like to thank all members of the Hayabusa2 mission team for their support of the data acquisition. All data will be available at the JAXA Data Archives and Transmission System (DARTS) at `https://www.darts.isas.jaxa.jp/planet/project/hayabusa2/`. This study is supported by the JSPS KAKENHI No. JP17H06459 ("Aqua Planetology") and the JSPS Core-to-Core Program "International Network of Planetary Sciences". We would like to thank Editage (www.editage.com) for English language editing.

References

Arakawa, M., Saiki, T., Wada, K., Ogawa, K., Kadono, T., Shirai, K., ... Miura, A. (2020). An artificial impact on the asteroid (162173) Ryugu formed a crater in the gravity-dominated regime. *Science*. doi: 10.1126/science.aaz1701

Benson, C. J., Scheeres, D. J., & Moskovitz, N. A. (2019). Spin state evolution of asteroid (367943) Duende during its 2013 earth flyby. *Icarus*, 113518. Retrieved from `http://www.sciencedirect.com/science/article/pii/S0019103519304075` doi: https://doi.org/10.1016/j.icarus.2019.113518

Bottke, W. F., Nolan, M. C., Greenberg, R., & Kolvoord, R. A. (1994). Velocity Distributions among Colliding Asteroids. *Icarus*, *107*(2), 255–268. doi: 10.1006/icar.1994.1021

Bottke, W. F., Vokrouhlický, D., Rubincam, D. P., & Nesvorný, D. (2006, may). THE

YARKOVSKY AND YORP EFFECTS: Implications for Asteroid Dynamics. *Annual Review of Earth and Planetary Sciences*, *34*(1), 157–191. Retrieved from http://www.annualreviews.org/doi/10.1146/annurev.earth.34.031405.125154 doi: 10.1146/annurev.earth.34.031405.125154

Breiter, S., Bartczak, P., Czekaj, M., Oczujda, B., & Vokrouhlický, D. (2009). The YORP effect on 25 143 Itokawa. *Astronomy and Astrophysics*, *507*(2), 1073–1081. doi: 10.1051/0004-6361/200912543

Breiter, S., Michalska, H., Vokrouhlický, D., & Borczyk, W. (2007). Radiation-induced torques on spheroids. *Astronomy and Astrophysics*, *471*(1), 345–353. doi: 10.1051/0004-6361:20077313

Čapek, D., & Vokrouhlický, D. (2004). The YORP effect with finite thermal conductivity. *Icarus*, *172*(2), 526–536. doi: 10.1016/j.icarus.2004.07.003

Cho, Y., Morota, T., Kanamaru, M., Takaki, N., Yumoto, K., Ernst, C. M., ... Sugita, S. (2021). Geologic History and Crater Morphology of Asteroid (162173) Ryugu. *Journal of Geophysical Research - Planets*. Retrieved from https://www.essoar.org/action/showAuthorDashboard?state=submitted doi: 10.1002/essoar.10506689.1

Efroimsky, M. (2001). Relaxation of wobbling asteroids and comets - Theoretical problems, perspectives of experimental observation. *Planetary and Space Science*, *49*(9), 937–955. doi: 10.1016/S0032-0633(01)00051-4

Gaskell, R., Barnouin-Jha, O., Scheeres, D., Mukai, T., Hirata, N., Abe, S., ... Kominato, T. (2006). Landmark Navigation Studies and Target Characterization in the Hayabusa Encounter with Itokawa. *AIAA/AAS Astrodynamics Specialist Conference and Exhibit*. doi: 10.2514/6.2006-6660

Gaskell, R. W., Barnouin-Jha, O. S., Scheeres, D. J., Konopliv, A. S., Mukai, T., Abe, S., ... Demura, H. (2008). Characterizing and navigating small bodies with imaging data. *Meteoritics & Planetary Science*, *43*(6), 1049–1061. Retrieved from https://onlinelibrary.wiley.com/doi/abs/10.1111/j.1945-5100.2008.tb00692.x doi: 10.1111/j.1945-5100.2008.tb00692.x

Golubov, O. (2017). Analytic Model for Tangential YORP. *The Astronomical Journal*, *154*(6), 238. doi: 10.3847/1538-3881/aa88ba

Golubov, O., & Krugly, Y. N. (2012). Tangential component of the YORP effect. *Astrophysical Journal Letters*, *752*(1). doi: 10.1088/2041-8205/752/1/L11

Golubov, O., Scheeres, D. J., & Krugly, Y. N. (2014). A three-dimensional model of tangential yorp. *Astrophysical Journal*, *794*(1). doi: 10.1088/0004-637X/794/1/22

Grott, M., Knollenberg, J., Hamm, M., Ogawa, K., Jaumann, R., Otto, K. A., ... Moussi-Soffys, A. (2019). *Low thermal conductivity boulder with high porosity identified on C-type asteroid (162173) Ryugu.* doi: 10.1038/s41550-019-0832-x

Hergenrother, C. W., Maleszewski, C. K., Nolan, M. C., Li, J. Y., Drouet d'Aubigny, C. Y., Shelly, F. C., ... Marty, B. (2019). The operational environment and rotational acceleration of asteroid (101955) Bennu from OSIRIS-REx observations. *Nature Communications*, *10*(1). doi: 10.1038/s41467-019-09213-x

Hirabayashi, M., Tatsumi, E., Miyamoto, H., Komatsu, G., Sugita, S., Watanabe, S.-i., ... Tsuda, Y. (2019). The Western Bulge of 162173 Ryugu Formed as a Result of a Rotationally Driven Deformation Process. *The Astrophysical Journal*, *874*(1), L10. doi: 10.3847/2041-8213/ab0e8b

Hirata, N., Morota, T., Cho, Y., Kanamaru, M., ichiro Watanabe, S., Sugita, S., ... ichi Iijima, Y. (2020). The spatial distribution of impact craters on Ryugu. *Icarus*, *338*. doi: 10.1016/j.icarus.2019.113527

Hirata, N., Namiki, N., Yoshida, F., Matsumoto, K., Noda, H., Senshu, H., ... ichiro Watanabe, S. (2021). Rotational effect as the possible cause of the east-west asymmetric crater rims on Ryugu observed by LIDAR data. *Icarus*. doi: 10.1016/j.icarus.2020.114073

Housen, K. R., & Holsapple, K. A. (2011). Ejecta from impact craters. *Icarus*, *211*(1), 856–875. doi: 10.1016/j.icarus.2010.09.017

Kaasalainen, M., Ďurech, J., Warner, B. D., Krugly, Y. N., & Gaftonyuk, N. M. (2007, mar). Acceleration of the rotation of asteroid 1862 Apollo by radiation torques. *Nature*, *446*(7134), 420–422. Retrieved from `http://www.nature.com/articles/nature05614` doi: 10.1038/nature05614

Kitazato, K., Milliken, R. E., Iwata, T., Abe, M., Ohtake, M., Matsuura, S., ... Tsuda, Y. (2019). The surface composition of asteroid 162173 Ryugu from Hayabusa2 near-infrared spectroscopy. *Science*, *364*(6437), 272–275. doi: 10.1126/science.aav7432

Lowry, S. C., Fitzsimmons, A., Pravec, P., Vokrouhlický, D., Boehnhardt, H., Taylor, P. A., ... Kusnirák, P. (2007). Direct detection of the asteroidal YORP effect. *Science*, *316*(5822), 272–274. doi: 10.1126/science.1139040

Lowry, S. C., Weissman, P. R., Duddy, S. R., Rozitis, B., Fitzsimmons, A., Green, S. F., ... van Oers, P. (2014). The internal structure of asteroid (25143) Itokawa as revealed by detection of YORP spin-up. *Astronomy & Astrophysics*, *562*, A48. Retrieved from https://doi.org/10.1051/0004-6361/201322602 doi: 10.1051/0004-6361/201322602

Michel, P., Ballouz, R.-L., Barnouin, O. S., Jutzi, M., Walsh, K. J., May, B. H., ... Lauretta, D. S. (2020, dec). Collisional formation of top-shaped asteroids and implications for the origins of Ryugu and Bennu. *Nature Communications*, *11*(1), 2655. Retrieved from http://www.nature.com/articles/s41467-020-16433-z doi: 10.1038/s41467-020-16433-z

Michikami, T., Honda, C., Miyamoto, H., Hirabayashi, M., Hagermann, A., Irie, T., ... Sugita, S. (2019). Boulder size and shape distributions on asteroid Ryugu. *Icarus*, *331*, 179–191. doi: 10.1016/j.icarus.2019.05.019

Morota, T., Sugita, S., Cho, Y., Kanamaru, M., Tatsumi, E., Sakatani, N., ... Tsuda, Y. (2020). Sample collection from asteroid (162173) Ryugu by Hayabusa2: Implications for surface evolution. *Science*, *368*(6491), 654–659. doi: 10.1126/science.aaz6306

Mysen, E. (2006). Canonical rotation variables and non-Hamiltonian forces: Solar radiation pressure effects on asteroid rotation. *Monthly Notices of the Royal Astronomical Society*, *372*(3), 1345–1350. doi: 10.1111/j.1365-2966.2006.10944.x

Mysen, E. (2008). *Dynamical effects of thermal emission on asteroids* (Vol. 383) (No. 1). doi: 10.1111/j.1745-3933.2007.00405.x

Noguchi, R., Hirata, N., Hirata, N., Shimaki, Y., Nishikawa, N., Tanaka, S., ... Watanabe, S.-i. (2021). Crater depth-to-diameter ratios on asteroid 162173 Ryugu d/D of craters on Ryugu. *Icarus*, *354*, 114016. Retrieved from http://www.sciencedirect.com/science/article/pii/S0019103520303791 doi: https://doi.org/10.1016/j.icarus.2020.114016

Nolan, M. C., Howell, E. S., Scheeres, D. J., McMahon, J. W., Golubov, O., Hergenrother, C. W., ... Lauretta, D. S. (2019). Detection of Rotational Acceleration of Bennu Using HST Light Curve Observations. *Geophysical Research Letters*, *46*(4), 1956–1962. doi: 10.1029/2018GL080658

Okada, T., Fukuhara, T., Tanaka, S., Taguchi, M., Arai, T., Senshu, H., ... Tsuda, Y. (2020). Highly porous nature of a primitive asteroid revealed by thermal imaging. *Nature*, *579*(7800), 518–522. doi: 10.1038/s41586-020-2102-6

Rozitis, B., & Green, S. F. (2011). Directional characteristics of thermal-infrared beaming from atmosphereless planetary surfaces - a new thermophysical model. *Monthly Notices* *of the Royal Astronomical Society*, *415* (3), 2042–2062. doi: 10.1111/j.1365-2966.2011.18718.x

Rozitis, B., & Green, S. F. (2012). The influence of rough surface thermal-infrared beaming on the Yarkovsky and YORP effects. *Monthly Notices of the Royal Astronomical Society*, *423* (1), 367–388. doi: 10.1111/j.1365-2966.2012.20882.x

Rubincam, D. P. (2000). Radiative Spin-up and Spin-down of Small Asteroids. *Icarus*, *148* (1), 2–11. doi: 10.1006/icar.2000.6485

Scheeres, D. J. (2007). The dynamical evolution of uniformly rotating asteroids subject to YORP. *Icarus*, *188* (2), 430–450. doi: 10.1016/j.icarus.2006.12.015

Scheeres, D. J. (2015). Landslides and Mass shedding on spinning spheroidal asteroids. *Icarus*, *247*, 1–17. doi: 10.1016/j.icarus.2014.09.017

Scheeres, D. J., Ostro, S. J., Werner, R. A., Asphaug, E., & Hudson, R. S. (2000). Effects of Gravitational Interactions on Asteroid Spin States. *Icarus*, *147* (1), 106–118. doi: 10.1006/icar.2000.6443

Ševeček, P., Golubov, O., Scheeres, D. J., & Krugly, Y. N. (2016, aug). Obliquity dependence of the tangential YORP. *Astronomy & Astrophysics*, *592*, A115. Retrieved from `http://www.aanda.org/10.1051/0004-6361/201628746` doi: 10.1051/0004-6361/201628746

Shimaki, Y., Senshu, H., Sakatani, N., Okada, T., Fukuhara, T., Tanaka, S., ... ichiro Watanabe, S. (2020). Thermophysical properties of the surface of asteroid 162173 Ryugu: Infrared observations and thermal inertia mapping. *Icarus*, *348*. doi: 10.1016/j.icarus.2020.113835

Statler, T. S. (2009). Extreme sensitivity of the YORP effect to small-scale topography. *Icarus*, *202* (2), 502–513. doi: 10.1016/j.icarus.2009.03.003

Sugita, S., Honda, R., Morota, T., Kameda, S., Sawada, H., Tatsumi, E., ... Tsuda, Y. (2019, mar). The geomorphology, color, and thermal properties of Ryugu: Implications for parent-body processes. *Science*, *364* (6437), eaaw0422. Retrieved from `https://www.sciencemag.org/lookup/doi/10.1126/science.aaw0422` doi: 10.1126/science.aaw0422

Szeliski, R. (2011). Computer vision: algorithms and applications. *Choice Reviews Online*, *48* (09), 48–5140–48–5140. doi: 10.5860/choice.48-5140

Tachibana, S., Abe, M., Arakawa, M., Fujimoto, M., Iijima, Y., Ishiguro, M., ... Kuninaka, H. (2014). Hayabusa2: Scientific importance of samples returned from C-type near-

Earth asteroid (162173) 1999 JU3. *Geochemical Journal*, *48*(6), 571–581. doi: 10.2343/geochemj.2.0350

Takita, J., Senshu, H., & Tanaka, S. (2017). *Feasibility and Accuracy of Thermophysical Estimation of Asteroid 162173 Ryugu (1999 JU3) from the Hayabusa2 Thermal Infrared Imager* (Vol. 208) (No. 1-4). doi: 10.1007/s11214-017-0336-x

Tatsumi, E., Domingue, D., Schröder, S., Yokota, Y., Kuroda, D., Ishiguro, M., ... Sugita, S. (2020). Global photometric properties of (162173) Ryugu. *Astronomy and Astrophysics*. doi: 10.1051/0004-6361/201937096

Tatsumi, E., & Sugita, S. (2018). Cratering efficiency on coarse-grain targets: Implications for the dynamical evolution of asteroid 25143 Itokawa. *Icarus*. doi: 10.1016/j.icarus.2017.09.004

Taylor, P. A., Margot, J. L., Vokrouhlický, D., Scheeres, D. J., Pravec, P., Lowry, S. C., ... Magri, C. (2007). Spin rate of asteroid (54509) 2000 PH5 increasing due to the YORP effect. *Science*, *316*(5822), 274–277. doi: 10.1126/science.1139038

Tsuda, Y., Yoshikawa, M., Saiki, T., Nakazawa, S., & ichiro Watanabe, S. (2019). Hayabusa2 Sample return and kinetic impact mission to near-earth asteroid Ryugu. *Acta Astronautica*, *156*, 387–393. doi: 10.1016/j.actaastro.2018.01.030

Vokrouhlický, D., & Čapek, D. (2002). Yorp-induced long-term evolution of the spin state of small asteroids and meteoroids: Rubincam's approximation. *Icarus*, *159*(2), 449–467. doi: 10.1006/icar.2002.6918

Watanabe, S., Hirabayashi, M., Hirata, N., Hirata, N., Noguchi, R., Shimaki, Y., ... Tsuda, Y. (2019). Hayabusa2 arrives at the carbonaceous asteroid 162173 Ryugu-A spinning top-shaped rubble pile. *Science*, *364*(6437), 268–272. doi: 10.1126/science.aav8032

Watanabe, S., Tsuda, Y., Yoshikawa, M., Tanaka, S., Saiki, T., & Nakazawa, S. (2017). *Hayabusa2 Mission Overview* (Vol. 208) (No. 1-4). doi: 10.1007/s11214-017-0377-1

Ďurech, J., Vokrouhlický, D., Baransky, A. R., Breiter, S., Burkhonov, O. A., Cooney, W., ... Warner, B. D. (2012). Analysis of the rotation period of asteroids (1865) Cerberus, (2100) Ra-Shalom, and (3103) Eger-search for the YORP effect. *Astronomy and Astrophysics*. doi: 10.1051/0004-6361/201219396

Ďurech, J., Vokrouhlický, D., Kaasalainen, M., Higgins, D., Krugly, Y. N., Gaftonyuk, N. M., ... Dyvig, R. R. (2008, oct). Detection of the YORP effect in asteroid (1620) Geographos. *Astronomy and Astrophysics*, *489*(2), L25–L28. Retrieved from `http://www.aanda.org/10.1051/0004-6361:200810672` doi: 10.1051/0004-6361:

200810672

Ďurech, J., Vokrouhlický, D., Kaasalainen, M., Weissman, P., Lowry, S. C., Beshore, E., ... Kitazato, K. (2008, sep). New photometric observations of asteroids (1862) Apollo and (25143) Itokawa - An analysis of YORP effect. *Astronomy and Astrophysics*, *488*(1), 345–350. Retrieved from http://www.aanda.org/10.1051/0004-6361:200809663 doi: 10.1051/0004-6361:200809663

Ďurech, J., Vokrouhlický, D., Pravec, P., Hanuš, J., Farnocchia, D., Krugly, Y. N., ... Warner, B. D. (2018, jan). YORP and Yarkovsky effects in asteroids (1685) Toro, (2100) Ra-Shalom, (3103) Eger, and (161989) Cacus. *Astronomy & Astrophysics*, *609*, A86. Retrieved from https://www.aanda.org/10.1051/0004-6361/201731465 doi: 10.1051/0004-6361/201731465